ACS APPLIED MATERIALS & INTERFACES

Research Article

www.acsami.org

Multifunctional Organic Phototransistor-based Nonvolatile Memory Achieved by UV/Ozone Treatment of the Ta_2O_5 Gate Dielectric

Xiaohui Liu, Haoyan Zhao, Guifang Dong,* Lian Duan, Dong Li, Liduo Wang, and Yong Qiu*

Key Laboratory of Organic Optoelectronics & Molecular Engineering of Ministry of Education, Department of Chemistry, Tsinghua University, Beijing 100084, China

Supporting Information

ABSTRACT: An organic phototransistor (OPT) shows nonvolatile memory effect due to its novel optical writing and electrical erasing processes. In this work, we utilize an organic light-emitting diode (OLED) as the light source to investigate OPT-based memory (OPTM) performance. It is found that the OPTM can be used as either flash memory or write-once read-many-times memory by adjusting the properties of the Ta_2O_5 gate dielectric layer. UV/ozone treatment is applied to effectively change dielectric properties of the Ta_2O_5 film. The mechanisms for this are examined by X-ray photoelectron spectroscopy and capacitance−voltage measurement. It turns out that the densities of oxygen vacancies and defects in the first 1.8 nm Ta_2O_5 films near the Ta_2O_5/semiconductor interface are reduced. Furthermore, for the first time, we use this multifunctional OPTM, which unites the photosensitive and memory properties in one single device, as an optical feedback system to tune the brightness of the OLED. Our study suggests that these OPTMs have potential applications in tuning the brightness uniformity, improving the display quality and prolonging the lifetime of flat panel displays.

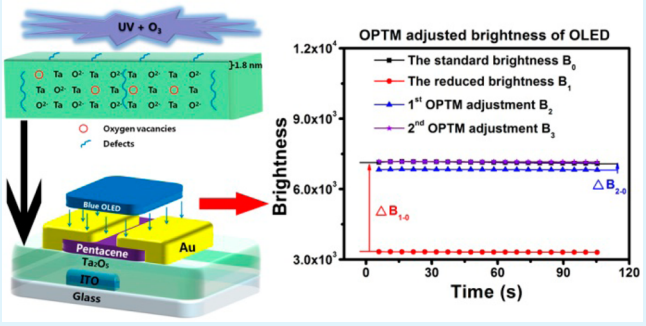

KEYWORDS: *organic phototransistor, nonvolatile memory, UV/ozone treatment, multifunctional applications*

1. INTRODUCTION

Organic electronic devices, such as organic solar cells, organic light emitting diodes (OLEDs), organic thin film transistors (OTFTs), and organic memory devices, keep attracting much attention due to their advantages such as being solution-processable, low-cost, lightweight, flexible, and large-area compatible. Intriguingly, functional OTFTs have broadened the research field and aroused great interest. For instance, some kinds of OTFTs show nonvolatile memory effects.[1−4] However, disadvantages such as high programming and erasing voltages and small ON/OFF current ratios have emerged. Moreover, new derivatives of OTFTs have also been reported, among which the organic phototransistor (OPT) stands out because it functions both in signal amplification and light detection.[5−11] In addition to the same three terminal configuration of OTFTs, OPTs possess a fourth terminal, light, to enable additional charge carriers and enhance the channel carrier density. The persistence of the photocurrent gives rise to data storage. With an electrical pulse, the recorded data can be erased as well. Then, a memory based on OPTs is completed with the special optical writing and electrical erasing processes.[12−24] Attributed to the aid of light illumination, the aforementioned disadvantages existing in traditional OTFT memories could be overcome by OPT-based memory (OPTM). Furthermore, with the integration of photosensitive and memory properties into one single device, the OPTM is promising for applications in photosensors, electronic eyes, etc. The multifunctional OPTM applications are in need of deep exploration.

Here, we find that the performance, including the photoresponsivity and memory window, of OPTM relies on two factors: (1) the interface states between the semiconductor and the gate dielectric and (2) the trap density in the gate dielectric. Both of them are essential for charge trapping and hence influence memory properties. For pentacene-based OPTs, the photoresponsivity is typically below 0.2 A W^{-1} when polymer dielectrics are used,[25−27] whereas the photoresponsivity can increase to near 1 A W^{-1} using SiO_2 gate dielectrics.[28,29] Moreover, Zan et al. report that the OPT with an UV treated polymer dielectric shows high photoresonsivity of about 10 A W^{-1}.[30] Therefore, it is crucial to choose an appropriate gate dielectric material and construct a desired interface for charge transport. Despite the fact that silicon dioxide is the most frequently used gate dielectric,[12,20−23] tantalum pentoxide (Ta_2O_5) may be a more suitable candidate for OPTM due to the large amount of electron trapping sites, which results in high photosensitivity[31] and a large memory window.[18] The origin of the electron trapping sites is associated with vacant Ta d orbits in Ta_2O_5, which could serve as electron acceptors.[32] Once the Ta_2O_5/pentacene interface forms, the electron

Received: February 27, 2014
Accepted: May 9, 2014
Published: May 9, 2014

trapping sites play a key role in the device performance. Our recent research based on Ta_2O_5 and Zan's group and Debucquoy's group has demonstrated that the interface between the semiconductor and the gate dielectric has a great effect on OPTM performance.[18,30,33] UV/ozone treatment is a facile method to tune the properties of Ta_2O_5 and the interface states. It is meaningful for the understanding of the possible mechanisms. More importantly, according to different device performances, multifunctional applications can be achieved.

In this study, we investigated the multifunctional OPTMs applications by adjusting the properties of the gate dielectric Ta_2O_5 and utilizing a blue OLED as the light source. By treating the Ta_2O_5 film with UV/ozone for 0, 10, 30, and 45 min, respectively, we successfully tuned the threshold voltage, currents, photoresponsivity, memory window, and retention time. The X-ray photoelectron spectroscopy depth profile of the Ta_2O_5 film and capacitance−voltage of the metal−insulator−semiconductor structure were measured and certified that the densities of oxygen vacancies and defects in the Ta_2O_5 film were reduced. Attributed to the result that the retention time of all devices were over 10^4 s, the OPTMs could be used as flash memory, write-once read-many-times memory and devices that could sense and feed back the brightness change of OLED displays. Herein, the multifunctional OPTM is a promising and potential organic photoelectronic device. We will present our study through the following three parts: (1) basic characteristics of OPTMs, (2) working mechanism of the UV/ozone treatment, and (3) the tuning of the multifunctional OPTM applications.

2. EXPERIMENTAL SECTION

2.1. Fabrication of OPTM Devices. A top-contact bottom-gate configuration was employed for device fabrication. Glass substrates well-patterned with 150 nm gate electrode indium tin oxide (ITO) were carefully cleaned in an ultrasonic bath and baked under an infrared bulb for 2 h before use. Then the substrate surface was UV/ozone cleaned for 10 min before any further deposition. Next, a 300 nm Ta_2O_5 gate dielectric film was sputtered on the substrate in an Ar/O_2 (1:1) gas mixture with a Φ101.6 × 7 mm target material Ta (General Research Institute for Nonferrous Metals, >99.9%). In particular, for the UV/ozone controlled experiments, the gate dielectric film was further treated in the UV/ozone cleaning machine for 10, 30, and 45 min, respectively. It should be noted that all of the films were not annealed. A pentacene (Sigma-Aldrich, >99%, used as received) film with a thickness of 45 nm was then thermally evaporated at room temperature at a deposition rate of 0.01−0.02 nm s^{-1} under a 1×10^{-4} Pa vacuum. Finally, a 45 nm thick gold film was deposited through shadow masks to get the desired pattern of the source and drain electrodes. The channel length (L) and width (W) were 80 and 1800 μm, respectively.

2.2. Characterizations. The capacitance per area (C_i) of gate dielectrics was obtained by measuring capacitance−frequency properties of ITO/Ta_2O_5/Au with an Agilent 4294A analyzer. The OPTM performance was measured by a Keithley 4200 semiconductor characterization system in air at room temperature. OLED with a peak wavelength at 462 nm was employed as the light source with an incident intensity of 15 mW cm^{-2}. The irradiation direction was from the top of the devices. X-ray photoelectron spectroscopy (XPS, Thermofisher, Escalab 250Xi) with depth profile was utilized to assess the surface states and bulk states of the TaO_x film. Al Kα (1487.02 eV) radiation was used to excite the photoeletrons from the samples. The ion gun type was Ar^+ with an ion gun energy of 3 keV. Devices with the structure ITO/Ta_2O_5/pentacene/Au were devised to acquire the capacitance−voltage characteristics with an HP 4284A precision LCR meter.

3. RESULTS AND DISCUSSION

3.1. Basic Characteristics of OPTM Devices. *3.1.1. Electrical Properties in Darkness.* The device structure and transfer characteristics in darkness are shown in Figure 1a,b,

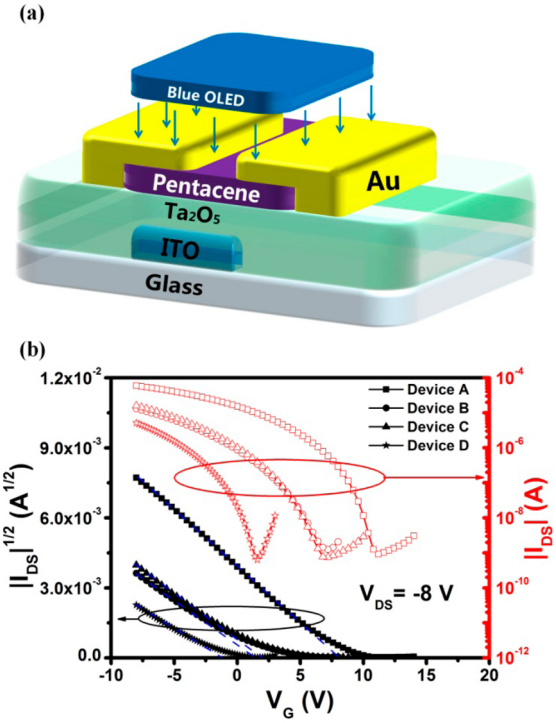

Figure 1. (a) Schematics of OPTM device structure. (b) Transfer curves of devices A, B, C, and D in darkness with V_{DS} = −8 V.

respectively. Before the evaporation of the pentacene layer, the Ta_2O_5 films of devices labeled A, B, C, and D received UV/ozone treatments for 0, 10, 30, and 45 min, respectively. The dielectric constant (ε) of the Ta_2O_5 films is calculated from the measured capacitance−frequency curves of the ITO/Ta_2O_5/Au structure (Supporting Information, Figure S1) at 100 kHz, whereas the leakage currents of the Ta_2O_5 films are shown in Figure S2 (Supporting Information). The field-effect mobility (μ) is extracted from the saturated region of the transfer curve. The threshold voltage (V_T), ON current (I_{ON}) and ON/OFF current ratio ($I_{ON/OFF}$) can be obtained in Figure 1b. The values of these five basic device parameters are listed in Table 1, among which the ε remained almost the same value, around 22, illustrating that UV/ozone treatment had little effect on the bulk states of the Ta_2O_5 film. However, the other four parameters exhibited a downward trend with increased UV/ozone treatment time. The field-effect mobility decreased after treatment, ranging from 0.1 to 0.3 cm^2 V^{-1} s^{-1}. A large negative shift of V_T from +7.8 to −1.2 V was observed, indicating that a blocking barrier for electron trapping was formed and that the trap density was reduced at or near the interface between pentacene and Ta_2O_5. As for device D, the negative V_T of −1.2 V could provide the device with an OFF state at V_G = 0, while the small value of V_T would reduce the power consumption with regards to application. The value of I_{ON} obtained at V_G = −8 V decreased about 1 order of magnitude compared with device A, which was consistent with the shift of V_T for the decrease of the value of $|V_G - V_T|$. It should be noted that there is no significant difference of performance between device

Table 1. Summary of the Fundamental Parameters of the UV/Ozone Treated Ta_2O_5-based OPTMs in Darkness: Channel Width/Length = 1800 μm/80 μm

	ε	μ (cm^2 V^{-1} s^{-1})	V_T (V)	I_{ON} (μA)	$I_{ON/OFF}$
device A	22.7	0.29 ± 0.07	7.9 ± 0.1	-52.8 ± 9	(6.7 ± 0.4) × 10^4
device B	22.0	0.16 ± 0.05	1.9 ± 0.1	-11.7 ± 2	(1.0 ± 0.3) × 10^4
device C	21.2	0.22 ± 0.03	1.3 ± 0.4	-14.0 ± 2	(2.3 ± 0.4) × 10^4
device D	22.1	0.12 ± 0.01	-1.2 ± 0.1	-5.31 ± 0.5	(0.51 ± 0.3) × 10^4

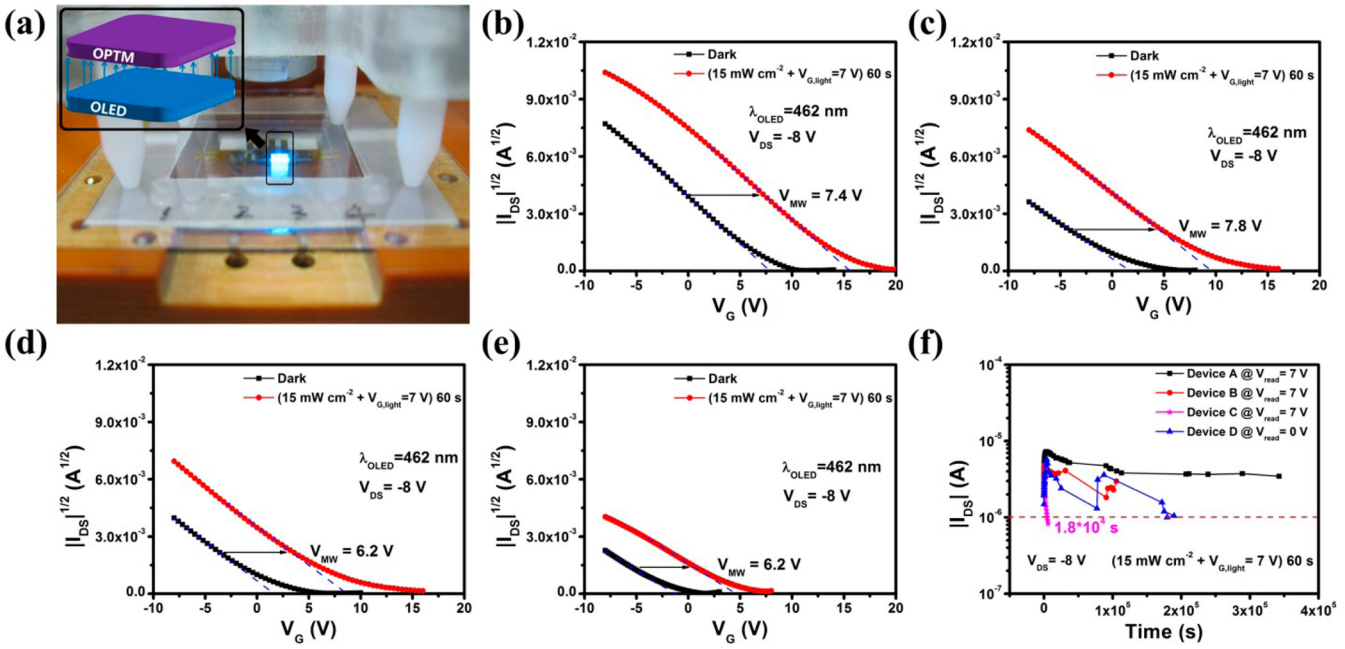

Figure 2. (a) Image of OPTM devices under the illumination of the blue OLED. The light was irradiated from the top of the OPTM. Panels b, c, d, and e refer to shift of the transfer curves after the optical writing process and in darkness for devices A, B, C, and D, respectively. (f) Retention time of OPTM devices.

B and device C, indicating that device performance would remain unchanged during a certain period of treatment time until a longer treatment time applied. Table 1 shows that the density of trapped electrons decreased as the treatment time prolonged.

3.1.2. Photosensitive and Memory Properties. The image of the testing system and the photosensitive and memory properties is depicted in Figure 2a. A blue OLED with an emission peak at 462 nm was selected as the light source, based on the relationship between the absorption spectrum of pentacene and the photocurrent.[34] As shown in Figure 2a, the blue bottom-emitting OLED with a power density of 15 mW cm^{-2} is placed below the OPTM. When the blue OLED is turned on, an additional gate voltage ($V_{G,light}$ = 7 V) is applied to assist the optical writing process for 60 s. Herein, the values of the photoresponsivity (R) and photocurrent/dark-current ratio (P) can be estimated by eqs 1 and 2, respectively, which are two important parameters for analyzing photosensitive properties in OPTs.

$$R = \frac{|I_{ill} - I_{dark}|}{P_{ill}} \quad (1)$$

$$P = \frac{|I_{ill} - I_{dark}|}{|I_{dark}|} \quad (2)$$

where P_{ill} is the incident power on the conducting channel, I_{ill} is the drain current under illumination, and I_{dark} is the drain current in darkness.

The memory window (V_{MW}) is defined as the shift of V_T from transfer curves in darkness (squares in Figure 2b–e) to those under illumination (circles in Figure 2b–e). In addition to V_{MW}, the retention time (t_R) is another criterion of the memory properties, defined as the time that the stored information dropped to a certain value (1 μA) at which a verifiable error is detected from any cause.[35]

Table 2 contains the maximum values of R and P (R_{max} and P_{max}) and the value of V_{MW} for each device. Obviously, with increased UV/ozone treatment time, the value of R_{max} decreased and device A had the highest R_{max} of 2.17 A W^{-1}. Although a sharp drop of R_{max} could be observed when the

Table 2. Photosensitive and Memory Properties of the UV/Ozone Treated Ta_2O_5-based OPTMs

	R_{max} (A W^{-1})[a]	P_{max}[a]	V_{MW} (V)[b]
device A	2.19 @ V_G = −6.4 V	2.8 × 10^3 @ V_G = 11.2 V	7.4
device B	2.17 @ V_G = −8 V	1.6 × 10^3 @ V_G = 6.8 V	7.8
device C	1.65 @ V_G = −8 V	1.6 × 10^3 @ V_G = 6.8 V	6.2
device D	0.58 @ V_G = −8 V	2.0 × 10^3 @ V_G = 1.6 V	6.2

[a]The photosensitive properties; V_G refers to the point the maximum value obtained. [b]The memory properties.

dx.doi.org/10.1021/am501197d | ACS Appl. Mater. Interfaces 2014, 6, 8337–8344

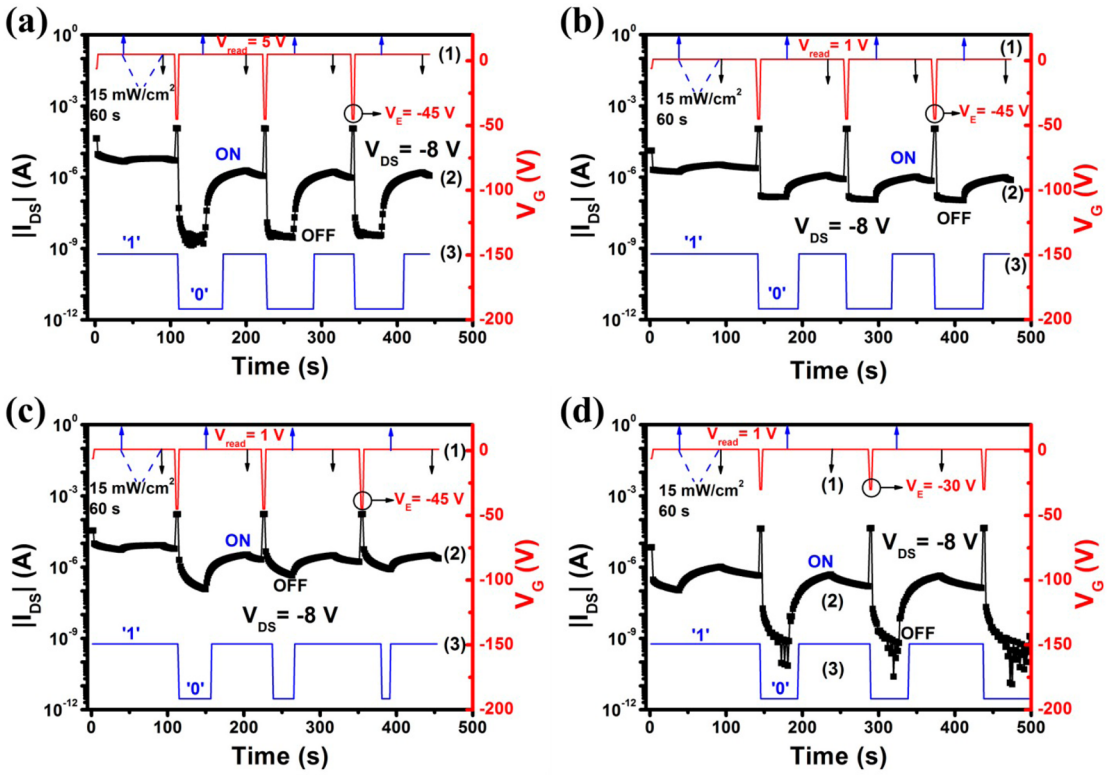

Figure 3. Optically-write-read-erase-read cycles of (a) device A, (b) device B, (c) device C, and (d) device D.

UV/ozone treatment time was increased to 45 min, the R_{max} of the other three devices significantly increased compared with previous reports.[18,25−29] It is noteworthy that P_{max} remained steadily at 10^3, obtained when $V_G \approx V_T$. On account of the same order of magnitude of the I_{DS} at $V_G \approx V_T$, it was proposed that devices A, B, C, and D had almost the same maximum amount of photocurrent. Generally, V_{MW} showed a tendency of reduction and the value decreased slowly from about 7 to 6 V, unfolding the increased blocking effect for the electron trapping process. In Figure 2f, I_{DS} is recorded with time after the devices underwent the optical writing process (blue OLED + $V_{G,light}$ = 7 V) for 60 s. The reading voltage (V_{read}) was set at 7 V for devices A, B, and C, while fixed at 0 V for device D. Because the I_{DS} value of device D was much smaller than the others when V_{read} = 7 V, to guarantee almost the same I_{DS} value of these four devices, a V_{read} = 0 V was chosen for device D. Whereas, the t_R of device D, namely 1.8×10^4 s, was still greatly shorter than that of the others. The t_R of device A was longer than that of both devices B and C, and all exceeded 10^5 s. Even so, the retention times of all these four devices were larger than we reported in ref 18 and sufficiently long for nonvolatile memory application. It appeared that the UV/ozone treatment had a deteriorative effect on device performance and the impact was significantly expanded when the treatment time was more than 45 min. Nevertheless, the overall performance of devices with 45 min of UV/ozone treatment was excellent for application in nonvolatile memory, especially with a V_T of −1.2 V, which was energy-saving and could ensure the OFF state of the device at 0 V.

For device A, the photosensitive and memory properties were measured utilizing OLEDs with different wavelengths including 544 and 628 nm (Supporting Information, Figure S3). In terms of V_{MW}, the value reduced when the wavelength of OLED was increased from 462 to 544 nm and further increased to 628 nm, which was in agreement with our previous report.[34]

The whole memory procedure consists of an optically-write-read-erase-read cycle. Lines (1) in Figure 3 are composed of a V_{read} with an interval of 1 s and a pulse erasing voltage (V_E) with a width of 3 s. During the reading process, the blue OLED was turned on for 60 s to complete the optical writing process and the blue upward and black downward arrows symbolized the points that the OLED was turned on and turned off, respectively. Hence, this meant that $V_{G,light}$ = V_{read} in the memory procedure. To achieve relatively similar initial currents, V_{read} = 5 V was chosen for device A while V_{read} = 1 V was fixed for the other three devices. With the consideration of different electrical endurance, the V_E value of device D was set to be −30 V, whereas the other three devices were applied at a same V_E of −45 V. Besides, the value of V_{DS} was fixed at −8 V during the memory process. Lines (2) in Figure 3 record the output currents I_{DS} during several memory cycles. It could be found that the I_{DS} reached the highest value after the optical writing process and then degraded due to the slow relaxation of trapped electrons back to the conducting channel. The lowest value of I_{DS} was attained after the electrical erasing process. These two states were defined as the ON state and OFF state of the OPTM, respectively. The ON/OFF current ratio of devices A and D was about 10^4, 3 orders of magnitude larger than that of both devices B and C. With a larger ON/OFF current ratio, the influence of the noise on the signal will become less. Lines (3) in Figure 3 are obtained from lines (2) using logic calculation. If the absolute value of I_{DS} is larger than a certain value, e.g., 10^{-6} A, then the result will be 1 and the else will be 0. It was advantageous to distinguish the ON and OFF states.

3.2. Working Mechanism of the UV/Ozone Treatment.

The results of section 3.1 demonstrated that the UV/ozone

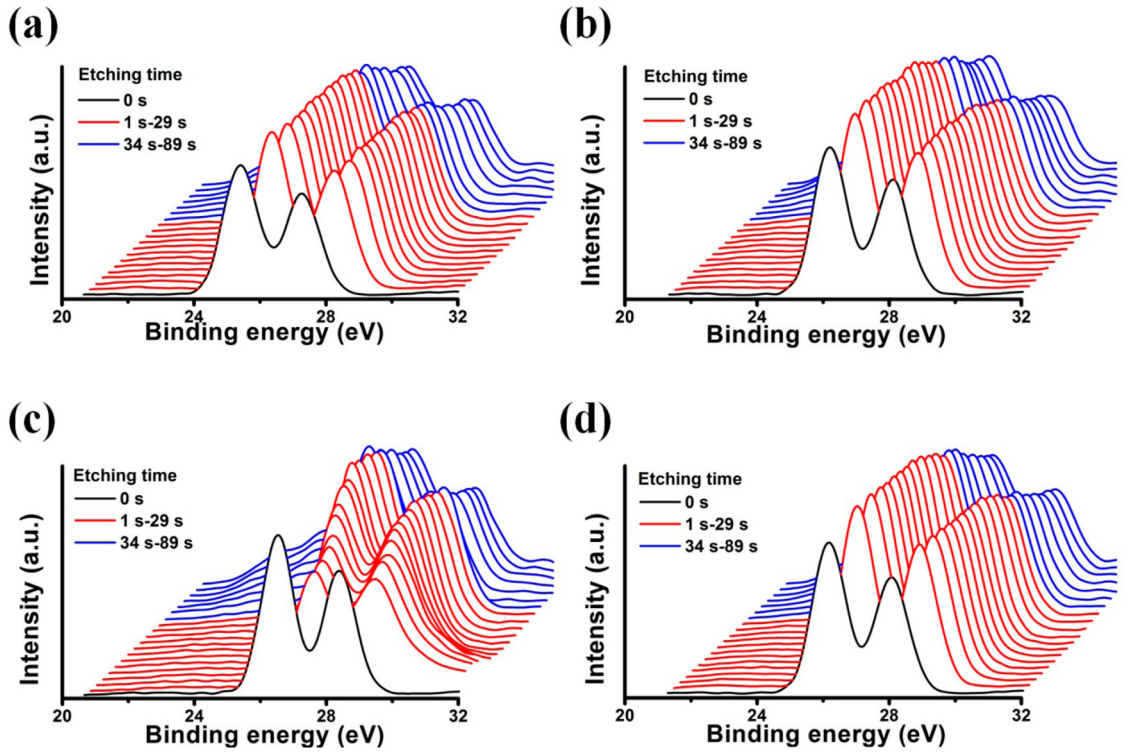

Figure 4. Ta 4f peaks of the XPS depth profiles of Ta_2O_5 film treated by UV/ozone for (a) 0, (b) 10, (c) 30, and (d) 45 min.

treatment greatly adjusted the characteristics of OPTMs. It should be related to the change of the Ta_2O_5 films. Then, the XPS depth profile of UV/ozone deposited Ta_2O_5 films was examined to investigate the oxidation states of Ta and their proportions (Figure 4).

The etching rate of the Ta_2O_5 film was determined to be 0.06 nm s^{-1}. All binding energies (E_B) were corrected for the sample charging effect with reference to the C 1s line at 284.8 eV. Further, to clearly distinguish the different oxidation states, the Ta peaks in XPS spectra were deconvoluted using a Gaussian-Lorentzian profile by standard software provided by the XPS system. The Ta 4f peak could be decomposed into some doublets. One doublet peak was composed of a Ta $4f_{7/2}$ peak and a Ta $4f_{5/2}$ peak. The binding energy difference and the intensity ratio between Ta $4f_{7/2}$ and Ta $4f_{5/2}$ peak were maintained at 1.91 eV and 4/3, respectively.

In Figure 4, increasing the etching depth of the Ta_2O_5 films resulted in a shift of E_B toward high energy region for all devices, demonstrating the change of the oxidation states of Ta. The detailed information on Ta $4f_{7/2}$ peak at different etching depth or with different etching time is summarized in Table 3 and Figures S4–S7 (Supporting Information).

At the surface of the Ta_2O_5 film, the Ta $4f_{7/2}$ peak of the doublet was located almost at E_B = 26.0 eV for all devices. It indicated a high oxidation state of Ta but not perfectly stoichiometric Ta_2O_5. The measured E_B of stoichiometric Ta_2O_5 is around 26.6 eV.[36] Interestingly, increasing the etching time to 29 s, the E_B of device A gradually remained at 26.6 eV, whereas that of the other three devices slowly increased and exceeded 27 eV. It elucidated a higher oxidation state of Ta, which was close to the stoichiometric Ta_2O_5. Additionally, the intensity of the main doublet peak increased from 65.4% to 82.2%, revealing that the oxygen vacancies and defects were gradually repaired by the UV/ozone treatment. Longer UV/ozone treatment times resulted in fewer oxygen vacancies and

Table 3. Binding Energy of Ta $4f_{7/2}$ of the Main Ta 4f Doublet Peak with Different Etching Time of Ta_2O_5 Film

	etching time (s)						
	0	1	2	3	14	29	area ratio of the main doublet peak (%)
device A	26.0	26.1	26.4	26.6	26.6	26.6	65.4
device B	26.2	26.8	26.9	27.0	27.0	27.1	78.9
device C	26.1	27.5	27.5	27.5	27.1	27.2	81.4
device D	26.2	26.8	27.1	27.1	27.2	27.3	82.2

defects. When the etching process proceeded further (Supporting Information, Figures S6 and S7), another tantalum suboxide appeared while the area ratio of the main doublet peak showed little fluctuation among these four kinds of devices. Thereby, 29 s was the time that a difference existed and the XPS curve of all devices tended to be the same after 29 s. The depth of the Ta_2O_5 film at this etching time was estimated to be 1.8 nm, which was the special region affected by UV/ozone treatment. The consequence was coherent with the conclusion that the UV/ozone treatment would repair the oxygen vacancy in the Ta_2O_5 film.[37,38] This repair was due to the reaction between vacancies and excited oxygen atoms generated by selectively in O_3 gas radiated by a mercury lamp.[37]

Except for the effect of the first 1.8 nm Ta_2O_5 films on the device performance, Figure 5 presents the capacitance–voltage (C–V) test of the metal–insulator–semiconductor (MIS) structure ITO/Ta_2O_5/pentacene/Au to demonstrate the change of trap density at or near the pentacene–Ta_2O_5 interface. Bias voltage first swept forwards from the negative region to the positive region and then swept backwards, contributing to a counterclockwise loop. The counterclockwise loop of the hysteresis in the C–V curves revealed an electron

dx.doi.org/10.1021/am501197d | ACS Appl. Mater. Interfaces 2014, 6, 8337–8344

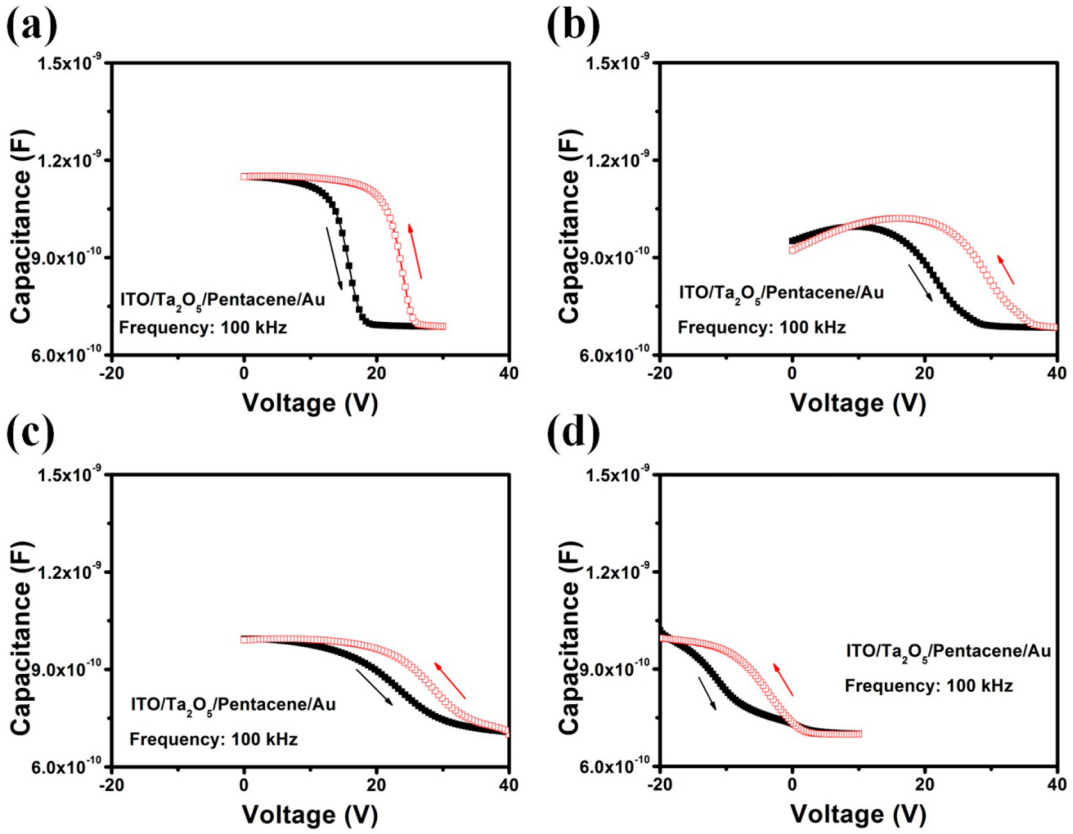

Figure 5. *C*−*V* characteristics of MIS structure ITO/Ta_2O_5/pentacene/Au on the basis of Ta_2O_5 with different UV/ozone treatment time: (a) 0 min with a voltage ranges from 0 to 30 V, (b) 10 min with a voltage ranges from 0 to 40 V, (c) 30 min with a voltage ranges from 0 to 40 V, and (d) 45 min with a voltage ranges from −20 to +10 V. The frequency was fixed at 100 kHz. Solid squares referred to sweeping direction from negative region to positive region while void squares referred to the reverse sweeping direction.

injection from pentacene to Ta_2O_5. It was noted that a decreasing hysteresis was observed from device A to device C. However, the hysteresis of device D became a little stronger than that of device C, which could be neglected. The hysteresis behavior was related to the trap density at the Ta_2O_5/pentacene interface or in the bulk Ta_2O_5 film, an analogical conclusion with the XPS analysis.

Hence, with UV/ozone treatment of Ta_2O_5 films, it was the reduction of the oxygen vacancies and trap density at or near the interface between pentacene and Ta_2O_5 that influenced the OPTM performances. The reduction of the oxygen vacancies and defects blocked the electron trapping process of the Ta_2O_5 film, leading to the decrease of mobile holes in the conducting channel, the negatively shifted V_T and hence the decrease of I_{ON} in darkness. Under illumination, the photogenerated excitons were easily dissociated into electrons and holes with the assist of $V_{G,light}$. Meanwhile, the electrons were trapped by the uncured defects in the Ta_2O_5 films, leading to the increase of charge carriers in the conducting channel. When the optical writing process ended, the trapped electrons were then released to pentacene again. However, it took a very long time to attain the original device performance in darkness. When a negative V_E was applied, the device could reach the OFF state immediately. Eventually, the photosensitive and memory properties were tuned as well.

3.3. Tuning of the Multifunctional OPTM Applications. After the analysis of the characteristics and work mechanism of OPTMs, we found the UV/ozone treatment time could tune the applications of OPTMs as well. In terms of nonvolatile memory, it can be classified as flash memory and write-once read-many-times memory. For devices A and D, the retention times were over 10^4 s, the ON/OFF current ratios were over 10^4, and the memory process could be achieved steadily for many times. Thus, devices A and D were appropriate for applications in flash memory. Even though devices B and C had long retention times, exceeding 10^5 s, the ON/OFF ratios were as low as 10 and degraded with the memory process. As a result, devices A and D could be applied in write-once read-many-times memory thanks to their long retention times. Obviously, it revealed the multifunctional applications of OPTMs.

Besides the above applications in memories, we propose our multifunctional OPTMs could be used in some novel applications because of the integrated photosensitive and memory properties. OPTMs could be adopted to sense the brightness of the flat panel display pixels, check out the aging pixels, modulate the reference currents for the aging pixels through a feedback circuit and then improve the brightness uniformity of the flat panel displays.

Figure 6 describes the adjustment process with one OPTM adjusting the brightness of one blue OLED pixel. The OLED was manipulated by an extra constant-voltage power supply. There were four states in this process, labeled states 0, 1, 2, and 3. In state 0, the OLED was applied with a constant voltage of 8 V and the corresponding brightness (B_0) was regarded as the standard brightness (square frames in Figure 6a). Squares in Figure 6b demonstrate the brightness versus time at 8 V. Illuminated by the blue OLED with the standard brightness, the

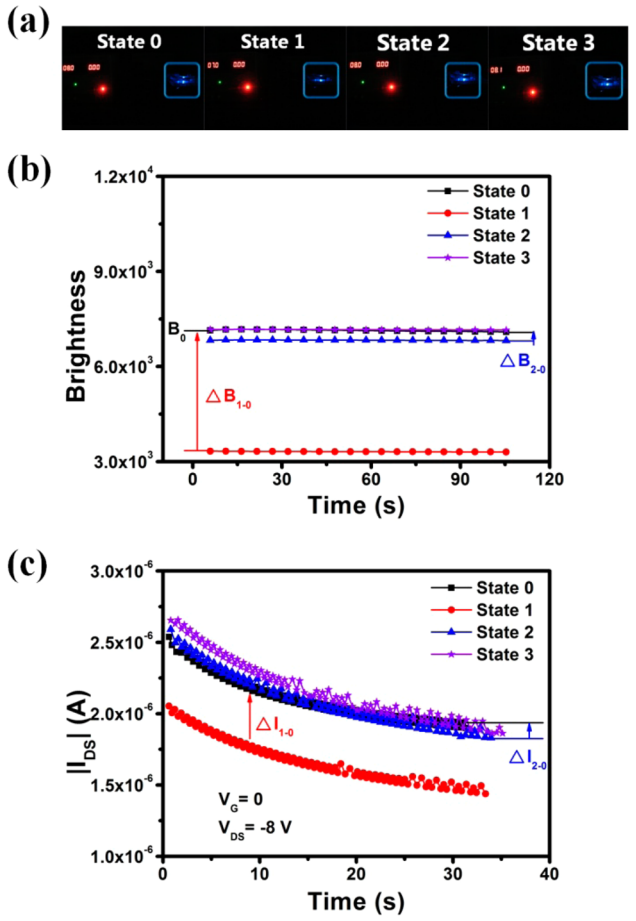

Figure 6. (a) Images of the blue OLED applied with different voltages in states 0, 1, 2, and 3. (b) $B-t$ curves of the blue OLED in states 0, 1, 2, and 3. (c) $I-t$ curves of OPTM device in states 0, 1, 2, and 3.

current of the OPTM was recorded with time at $V_G = 0$ and $V_{DS} = -8$ V (squares in Figure 6c) and thought to be the standard current (I_0).

To simulate the aging of the pixels, here we deliberately reduced the applied voltage of OLED from 8 to 7 V. Then the brightness of the OLED declined to state 1 (Figure 6a,b) and the decrease of I_{DS} was sensitively detected (Figure 6c). $\Delta I_{1\text{-}0}$ produced between state 1 and state 0 quantitatively denoted the difference of the brightness ($\Delta B_{1\text{-}0}$). In this situation, with the feedback circuit, the reference current for the pixel will be increased to tune the brightness of the OLED back to the standard value B_0. Here we adjusted the applied voltage to 8 V. However, a small $\Delta I_{2\text{-}0}$ still existed in the time range between 20 and 35 s in Figure 6c, illustrating that the degradation of the OLED performance had emerged. The brightness of state 2 in Figure 6b also proves the phenomenon of the degradation.

Finally, when we applied a voltage of 8.1 V on the OLED, the system reached state 3. In this state, the current of the OPTM nearly overlapped with the standard I_0, elucidating the successful modulation of the brightness. In Figure 6b, the stars note that the brightness of the OLED is tuned to its standard B_0.

Although we just utilized one OPTM to modulate the brightness of one OLED pixel, it pioneers a new application of OPTMs to improve the display quality and prolong the lifetime of OLED pixels. Additionally, it has promise for applications in the modulation of flat panel displays.

4. CONCLUSIONS

We successfully fabricated multifunctional OPTMs by UV/ozone treating the Ta_2O_5 insulating layer. It was demonstrated that the threshold voltage, current, photoresponsivity, and memory window were tuned by the UV/ozone treatment. XPS depth profiles and $C-V$ characteristics were measured to confirm that property changes, including oxygen vacancies and traps, of this 1.8 nm ultrathin film, originated from different treatment times, determined device performance. Furthermore, almost all the devices showed nonvolatile memory effect with a $t_R > 10^5$ s. On account of this, OPTM devices could be used as either flash memory or write-once read-many-times memory according to their different performances. In addition, because of the integration of the photosensitive and memory properties into one single device, the OPTM device was first used to modulate the brightness of the OLED. It paves the way to a new application for OPTMs to modulate brightness uniformity, improve display quality, and prolong lifetime of flat panel displays.

■ ASSOCIATED CONTENT

Supporting Information

Capacitance–frequency characteristics of ITO/Ta_2O_5/Au structure, leakage current of Ta_2O_5 films, transfer curves of device A exposed to OLED with peak emission at 544 and 628 nm, and detailed XPS fitting curves of Ta 4f with etching times of 0, 29, 34, and 89 s. This material is available free of charge via the Internet at http://pubs.acs.org.

■ AUTHOR INFORMATION

Corresponding Authors

*G. Dong. E-mail: donggf@mail.tsinghua.edu.cn. Tel: 86-10-6278 2287. Fax: 86-10-6279 5137.

*Y. Qiu. E-mail: qiuy@mail.tsinghua.edu.cn. Tel: 86-10-6278 2287. Fax: 86-10-6279 5137.

Notes

The authors declare no competing financial interest.

■ ACKNOWLEDGMENTS

This work is financially supported by the National Natural Science Foundation of China (No. 61177023, 51173096, and 21161160447).

■ REFERENCES

(1) Zhou, Y.; Han, S. T.; Xu, Z. X.; Roy, V. A. L. The Strain and Thermal Induced Tunable Charging Phenomenon in Low Power Flexible Memory Arrays with a Gold Nanoparticle Monolayer. *Nanoscale* **2013**, *5*, 1972–1979.

(2) Hsu, J. C.; Lee, W. Y.; Wu, H. C.; Sugiyama, K.; Hirao, A.; Chen, W. C. Nonvolatile Memory Based on Pentacene Organic Field-Effect Transistors with Polystyrenepara-Substituted Oligofluorene Pendent Moieties as Polymer Electrets. *J. Mater. Chem.* **2012**, *22*, 5820–5827.

(3) Chou, Y. H.; Lee, W. Y.; Chen, W. C. Self-Assembled Nanowires of Organic n-Type Semiconductor for Nonvolatile Transistor Memory Devices. *Adv. Funct. Mater.* **2012**, *22*, 4352–4359.

(4) She, X. J.; Liu, C. H.; Sun, Q. J.; Gao, X.; Wang, S. D. Morphology Control of Tunneling Dielectric towards High-Performance Organic Field-Effect Transistor Nonvolatile Memory. *Org. Electron.* **2012**, *13*, 1908–1915.

(5) Yu, H.; Bao, Z. N.; Oh, J. H. High-Performance Phototransistors Based on Single-Crystalline n-Channel Organic Nanowires and Photogenerated Charge-Carrier Behaviors. *Adv. Funct. Mater.* **2013**, *23*, 629–639.

(6) Tomoyuki, K.; Hirotaka, K.; Tadashi, K.; Takehiko, M. Giant Phototransistor Response in Dithienyltetrathiafulvalene Derivatives. *J. Mater. Chem. C* **2013**, *1*, 2900−2905.
(7) Wu, Y. C.; Yin, Z. Y.; Xiao, J. C.; Liu, Y.; Wei, F. X.; Tan, K. J.; Kloc, C.; Huang, L.; Yan, Q. Y.; Hu, F. Z.; Zhang, H.; Zhang, Q. C. Crystal Structure and Phototransistor Behavior of N-Substituted Heptacence. *ACS Appl. Mater. Interfaces* **2012**, *4*, 1883−1886.
(8) Sun, Z. H.; Li, J. H.; Yan, F. Highly Sensitive Organic Near-Infrared Phototransistors Based on Poly(3-hexylthiophene) and PbS Quantum Dots. *J. Mater. Chem.* **2012**, *22*, 21673−21678.
(9) Sun, Z. H.; Liu, Z. K.; Li, J. H.; Tai, G. A.; Lau, S. P.; Yan, F. Infrared Photodetectors Based on CVD-Grown Graphene and PbS Quantum Dots with Ultrahigh Responsivity. *Adv. Mater.* **2012**, *24*, 5878−5883.
(10) Guo, Y. L.; Du, C. Y.; Yu, G.; Di, C. A.; Jiang, S. D.; Xi, H. X.; Zheng, J.; Yan, S. K.; Yu, C. L.; Hu, W. P.; Liu, Y. Q. High-Performance Phototransistors Based on Organic Microribbons Prepared by a Solution Self-Assembly Process. *Adv. Funct. Mater.* **2010**, *20*, 1019−1024.
(11) Ahmed, R.; Kadashchuk, A.; Simbrunner, C.; Schwabegger, G.; Havlicek, M.; Glowacki, E.; Sariciftci, N. S.; Baig, M. A.; Sitter, H. Photosensitivity of Top Gate C60 Based OFETs: Potential Applications for High Efficiency Organic Photodetector. *Org. Electron.* **2014**, *15*, 175−181.
(12) Cho, M. Y.; Kim, S. J.; Han, Y. D.; Park, D. H.; Kim, K. H.; Choi, D. H.; Joo, J. Highly Sensitive, Photocontrolled, Organic Thin-Film Transistors Using Soluble Star-shaped Conjugated Molecules. *Adv. Funct. Mater.* **2008**, *18*, 2905−2912.
(13) Qi, Z.; Liao, X. X.; Zheng, J. C.; Di, C. A.; Gao, X. K.; Wang, J. Z. High-Performance n-Type Organic Thin-Film Phototransistors Based on a Core-Expanded Naphthalene Diimide. *Appl. Phys. Lett.* **2013**, *103*, 053301.
(14) Kim, K. H.; Bae, S. Y.; Kim, Y. S.; Hur, J. A.; Hoang, M. H.; Lee, T. W.; Cho, M. J.; Kim, Y.; Kim, M.; Jin, J. I.; Kim, S. J.; Lee, K.; Lee, S. J.; Choi, D. H. Highly Photosensitive J-Aggregated Single-Crystalline Organic Transistors. *Adv. Mater.* **2011**, *23*, 3095−3099.
(15) Debucquoy, M.; Verlaak, S.; Stoedel, S.; Vusser, S.; Genoe, J.; Heremans, P. Pentacene Organic Field-Effect Phototransistor with Memory Effect. *Proc. SPIE−Int. Soc. Opt. Eng.* **2006**, *6192*, 61921F.
(16) Baeg, K. J.; Noh, Y. Y.; Ghim, J.; Kang, S. J.; Lee, H.; Kim, D. Y. Organic Non-Volatile Memory Based on Pentacene Field-Effect Transistors Using a Polymeric Gate Electret. *Adv. Mater.* **2006**, *18*, 3179−3183.
(17) Zhang, L.; Wu, T.; Guo, Y. L.; Zhao, Y.; Sun, X. N.; Wen, Y. G.; Yu, G.; Liu, Y. Q. Large-Area, Flexible Imaging Arrays Constructed by Light-Charge Organic Memories. *Sci. Rep.* **2013**, *3*, 1080.
(18) Liu, X. H.; Dong, G. F.; Duan, L.; Wang, L. D.; Qiu, Y. High Performance Low-Voltage Organic Phototransistors: Interface Modification and the Tuning of Electrical, Photosensitive and Memory Properties. *J. Mater. Chem.* **2012**, *22*, 11836−11842.
(19) Mukherjee, B.; Mukherjee, M.; Choi, Y.; Pyo, S. Control over Multifunctionality in Optoelectronic Device Based on Organic Phototransistor. *ACS Appl. Mater. Interfaces* **2010**, *2*, 1614−1620.
(20) Zan, H. W.; Kao, S. C. New Organic Phototransistor with Bias-Modulated Photosensitivity and Bias-Enhanced Memory Effect. *IEEE Electron Dev. Lett.* **2009**, *30*, 721−723.
(21) Barra, M.; Bloisi, F.; Cassinese, A.; Girolamo, F. V.; Vicari, L. Photoinduced Long-Term Memory Effects in n-Type Organic Perylene Transistors. *J. Appl. Phys.* **2009**, *106*, 126105.
(22) Guo, Y. L.; Di, C. A.; Ye, S. H.; Sun, X. N.; Zheng, J.; Wen, Y. G.; Wu, W. P.; Yu, G.; Liu, Y. Q. Multibit Storage of Organic Thin-Film Field-Effect Transistors. *Adv. Mater.* **2009**, *21*, 1954−1959.
(23) Mas-Torrent, M.; Hadley, P.; Crivillers, N.; Veciana, J.; Rovira, C. Large Photoresponsivity in High-Mobility Single-Crystal Organic Field-Effect Phototransistors. *ChemPhysChem* **2006**, *7*, 86−88.
(24) Dutta, S.; Narayan, K. S. Gate-Voltage Control of Optically-Induced Charges and Memory Effects in Polymer Field-Effect Transistors. *Adv. Mater.* **2004**, *16*, 2151−2155.
(25) Dao, T. T.; Matsushima, T.; Murakami, M.; Ohkubo, K.; Fukuzumi, S.; Murata, H. Enhancement of Ultraviolet Light Responsivity of a Pentacene Phototransistor by Introducing Photoactive Molecules into a Gate Dielectric. *Jpn. J. Appl. Phys.* **2014**, *53*, 02BB03.
(26) Loffredo, F.; Bruno, A.; Mauro, A.; Grimaldi, I. A.; Miscioscia, R.; Nenna, G.; Pandolfi, G.; Petrosino, M.; Villani, F.; Minarini, C.; Facchetti, A. Photoresponse of Pentacene-Based Transistors. *Phys. Status Solidi A* **2014**, *211*, 460−466.
(27) Yang, D.; Zhang, L.; Yang, S. Y.; Zou, B. S. Influence of the Dielectric PMMA Layer on the Detectivity of Pentacene-Based Photodetector with Field-Effect Transistor Configuration in Visible Region. *IEEE Photonics J.* **2013**, *5*, 6801709.
(28) Noh, Y. Y.; Kim, D. Y. Organic Phototransistor Based on Pentacene as an Efficient Red Light Sensor. *Solid-State Electron.* **2007**, *51*, 1052−1055.
(29) Okur, S.; Yakuphanoglu, F.; Stathatos, E. High-Mobility Pentacene Phototransistor with Nanostructured SiO_2 Gate Dielectric Synthesized by Sol−Gel Method. *Microelectron. Eng.* **2010**, *87*, 635−640.
(30) Zan, H. W.; Yen, K. H. High Photoresponsivity of Pentacene-Based Organic Thin-Film Transistors with UV-Treated PMMA Dielectrics. *Electrochem. Solid-State Lett.* **2008**, *11*, H222−H225.
(31) Liang, Y.; Dong, G. F.; Hu, Y.; Wang, L. D.; Qiu, Y. Low-Voltage Pentacene Thin-Film Transistors with Ta_2O_5 Gate Insulators and Their Reversible Light-Induced Threshold Voltage Shift. *Appl. Phys. Lett.* **2005**, *86*, 132101.
(32) Johnson, R. S.; Hong, J. G.; Lucovsky, G. Electron Traps at Interfaces between Si (100) and Noncrystalline Al_2O_3, Ta_2O_5, and $(Ta_2O_5)_x$ $(Al_2O_3)_{1-x}$ Alloys. *J. Vac. Sci. Technol., B: Microelectron. Nanometer Struct.−Process., Meas., Phenom.* **2001**, *19*, 1606−1610.
(33) Debucquoy, M.; Verlaak, S.; Stoedel, S.; Myny, K.; Genoe, J.; Heremans, P. Organic Phototransistor Behavior and Light-Accelerated Bias Stress. *Proc.SPIE−Int. Soc. Opt. Eng.* **2007**, *6658*, 66580R.
(34) Hu, Y.; Dong, G. F.; Wang, L. D.; Qiu, Y. Phototransistor Properties of Pentacene Organic Transistors with Poly(methyl methacrylate) Dielectric Layer. *Jpn. J. Appl. Phys.* **2006**, *45*, L96−L98.
(35) *IEEE Standard for Definitions, Symbols, and Characterization of Floating Gate Memory Arrays*; 1005-1998; IEEE: New York, 1999.
(36) Lecuyer, S.; Quemerais, A.; Jezequel, G. Composition of Natural Oxide Films on Polycrystalline Tantalum Using XPS Electron Take-off Angle Experiments. *Surf. Interface Anal.* **1992**, *18*, 257−261.
(37) Shinriki, H.; Nakata, M. UV-O_3 and dry-O_2: Two-Step-Annealed Chemical Vapor-Deposited Ta_2O_5 Films for Storage Dielectrics of 64-Mb DRAMs. *IEEE Trans. Electron Devices* **1991**, *38*, 455−462.
(38) Xia, G. D.; Wang, S. M.; Zhao, X. R.; Zhou, L. M. High-Performance Low-Voltage Organic Transistor Memories with Room-Temperature Solution-Processed Hybrid Nanolayer Dielectrics. *J. Mater. Chem. C* **2013**, *1*, 3291−3296.